# The design of electroabsorption modulators with negative chirp and very low insertion loss

Kambiz Abedi†

Department of Electrical Engineering, Faculty of Electrical and Computer Engineering, Shahid Beheshti University, G. C., Evin 1983963113, Tehran, Iran

**Abstract:** Electroabsorption modulators (EAMs) with negative chirp and very low insertion loss are numerically designed with asymmetric intra-step-barrier coupled double strained quantum wells (AICD-SQWs) based on InGaAlAs material. For this purpose, the electroabsorption coefficient is calculated over a range of wells layer strain from compressive (CS) to tensile (TS). The chirp parameter and insertion loss for TE input light polarization are evaluated from the calculated electroabsorption spectra, and their Kramers–Krönig transformed refractive index changes. The results of the numerical simulation show that the best range of left and right wells strain for EAMs based on AICD-SQWs with negative chirp and very low insertion loss are from 0.032% to 0.05% (TS) and −0.52% to −0.50% (CS), respectively.

**Key words:** electroabsorption modulators; AICD-SQW; strain; chirp; insertion loss
**DOI:** 10.1088/1674-4926/33/6/064001 **EEACC:** 4200

## 1. Introduction

Electroabsorption modulators (EAMs) are among the most important components of fiber-optical communication devices and systems, because of their small size, low driving voltage, low chirp, high extinction ratio, high modulation efficiency, and wide modulation bandwidth. In addition, due to matching of material systems, EAMs can be easily integrated with other optical components, such as semiconductor lasers, semiconductor optical amplifiers, and attenuators, in contrast to modulators made in for instance $LiNbO_3$[1, 2].

For the long-haul high-speed fiber optic communication system typically working at a 1.55 $\mu$m wavelength, the product of the square of the bit rate and the transmission distance is limited by the modulator's chirp parameter and the fiber dispersion[3, 4]. The fiber dispersion will broaden the signal pulse width when the modulated light signal travels through the optical fiber. As the transmission distance increases, the pulse width will keep broadening and eventually become indistinguishable by the receiver, therefore bit error happens. To compensate the fiber dispersion of the conventional single mode fiber and to achieve wider bandwidth or higher bit rate optical signal transmission, EAMs with negative chirp parameter are desirable. However, most multiple-quantum-well EAMs generate positive chirp parameters. As a result, the reduction of chirp parameter without the outlay of a low insertion loss and high extinction ratio is an important issue for EAMs with both asymmetric and strained layer quantum wells[5−12].

An AICD-SQW structure in the active region has become the structure of choice for EAMs due to their improved extinction ratio and reduced insertion loss and chirp through applied strain, in comparison with the intra-step-barrier quantum well (IQW) structure[13−16]. With this new AICD-SQW, we analyzed chirp parameter and insertion loss with 0.05% tensile and 0.52% compressive strains for the left and right wells, respectively. The tensile and compressive strains in the AICD-SQW resulted in a zero chirp parameter[13]. This paper intends to investigate the effects of strain in the well layers on the chirp parameter and the insertion loss in the AICD-SQWs. The simulation results show that negative chirp and very low insertion loss can be achieved simultaneously.

## 2. The asymmetric intra-step-barrier coupled double strained quantum well structure

A schematic conduction band diagram of the active region for the AICD-SQW structure is shown in Fig. 1[13]. The undoped AICD-SQW structure consists of 100 Å $In_{0.52}Al_{0.48}As$ barriers and a 40 Å $In_{0.53}Ga_{0.33}Al_{0.14}As$ intra-step-barrier, which are lattice matched to InP. The asymmetric coupled wells system consists of a $In_{1-x_l-y_l}Ga_{x_l}Al_{y_l}As$ left well and a $In_{1-x_r-y_r}Ga_{x_r}Al_{y_r}As$ right well, separated from each other by 15 Å thick $In_{0.52}Al_{0.48}As$ as the narrow barrier. The thicknesses of the left and right wells are taken to be 68 and 35 Å, respectively. The direction of a positive electric field $F$ is defined as shown in Fig. 1.

Using ternary well materials, we extract the strain effect of the well layers on the chirp parameter without varying the quantum confinement effect. The modulator length and optical confinement factor are taken to be 200 $\mu$m and 0.15, respectively[14].

## 3. The electroabsorption spectrum

The field-dependent absorption spectrum $\alpha(h\nu)$ of the AICD-SQW structure, as shown in Fig. 1, is related to the imaginary part of the dielectric constant, $\varepsilon_i(h\nu)$, given as[13]

$$\alpha(h\nu) = \frac{2\pi}{\lambda_0 n_r}\varepsilon_i(h\nu) = \frac{\omega}{cn_r}\varepsilon_i(h\nu), \quad (1)$$

† Corresponding author. Email: k_abedi@sbu.ac.ir
Received 9 November 2011, revised manuscript received 9 February 2012

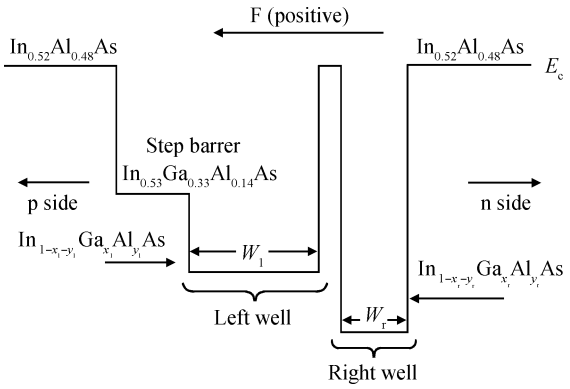


Fig. 1. AICD-SQW conduction band diagram.

where $\lambda_0$, $c$, and $n_r$ are the free-space wavelength of incident light, the speed of light in vacuum, and the refractive index, respectively. $\alpha(h\nu)$ in Eq. (1) can be defined as:

$$\alpha(h\nu) = \alpha(h\nu)^{\text{band}} + \alpha(h\nu)^{\text{exciton}}. \tag{2}$$

The first term is due to the band-to-band transitions and the second term is due to the excitonic transitions. The electroabsorption coefficient of the band-to-band transitions between $n$th subband electrons and $m$th subband holes is written as:

$$\alpha(h\nu)^{\text{band}} = \frac{e^2}{\varepsilon_0 m_0^2 c n_r \omega L_z}\frac{\mu}{\hbar^2}\int M_{nm}^2(E) \times L(h\nu - E - E_g - E_n^e - E_m^h)\mathrm{d}E, \tag{3}$$

where $\varepsilon_0$ is the dielectric constant, $m_0$ the free-electron mass, $L_z$ the effective thickness of the AICD-SQW, $E_g$ the energy gap, $\mu$ the reduced mass for the motion in the $xy$ plane, and $\hbar$ the reduced Planck constant, respectively. Here, we assume $L(y)$ to be a Lorentzian line shape function with a zero-field FWHM of 10 meV.

The quantity $M_{nm}(E)$ is $(\xi p_{cv})\,|I_{nm}|$, where $\xi$ is the polarization vector, $P_{CV}$ is the momentum matrix element between the conduction band and valence band Bloch functions, and $|I_{nm}|$ is the overlap integral between the conduction and valence subbands wave functions.

$E_n^e(k)$ and $E_m^h(k)$ are the electron and hole energy levels and wave functions, respectively, calculated by the TMM solution for the AICD-SQW structure[15].

For the calculation of the contribution of exciton transitions between the $n$th subband electron and the $m$th subband hole, the exciton equation in momentum space is solved numerically using the Gaussian quadrature method for 1s exciton state[13].

The exciton oscillator strength for this state is defined as:

$$f_X = \frac{2}{m_0 E_X}\left|\int \frac{d^2k}{(2\pi)^2}\phi_{nm}^X(k)M_{nm}(k)\right|^2, \tag{4}$$

where $\phi_{nm}^X(k)$ is the exciton envelope wave function in momentum space and $E_X$ is the transition energy for the 1s exciton state. The exciton binding energy is given by

$$E_B = E_X - E_n^e - E_m^h - E_g. \tag{5}$$

So, the electroabsorption coefficient of an exciton transition is written as

$$\alpha(h\nu)^{\text{exciton}} = \frac{\pi e^2\hbar}{n_r\varepsilon_0 m_0 c L_z}\sum_X f_X L(h\nu - E_X). \tag{6}$$

## 4. Frequency chirp and chirp parameter

Chirp can eventually limit the transmission performance due to the accompanied dynamic spectral broadening. The frequency chirp of an optical modulator makes reference to the instantaneous variation of the optical carrier frequency upon intensity modulation for a modulated lightwave[17].

The frequency chirp of the modulator output is determined from the time varying phase of the output optical field by

$$\Delta\nu(t) = \frac{1}{2\pi}\frac{\mathrm{d}\phi(t)}{\mathrm{d}t}. \tag{7}$$

For a dielectric material, its optical properties can be characterized by its complex refractive index, $n_r - \mathrm{j}n_i$. In EAMs, light modulation is through the change in absorption coefficient, i.e. the change in the imaginary part of the refractive index, $n_i$.

The imaginary part of the refractive index, $n_i(t)$, is related to the power absorption coefficient of the modulator, $\alpha(t)$,

$$n_i(t) = \frac{\lambda_0}{4\pi}\alpha(t). \tag{8}$$

The change in the phase of the output optical field with time leads to the instantaneous frequency shift, i.e. frequency chirp,

$$\Delta\nu(t) = \frac{1}{2\pi}\frac{\mathrm{d}\phi(t)}{\mathrm{d}t} = \frac{1}{2\pi}\frac{\alpha_H}{2I_{out}(t)}\frac{\mathrm{d}I_{out}(t)}{\mathrm{d}t}, \tag{9}$$

where $I_{out}(t)$ is the intensity of the output optical field. Therefore, the frequency chirp of an optical intensity modulator is characterized by the chirp parameter, which is defined as the ratio of the changes in the real part of refractive index, $n_r$, and the imaginary part, $n_i$, of the electroabsorption active layer due to an applied voltage. Thus, the chirp parameter $\alpha_H$ of the EAM is defined by

$$\alpha_H = \frac{\Delta n_r}{\Delta n_i} = \frac{4\pi}{\lambda_0}\frac{\Delta n_r}{\Delta\alpha}. \tag{10}$$

In principle, the change in the real refractive index $\Delta n_r$ can be obtained from the change in absorption coefficient $\Delta\alpha$ by the Kramers–Kronig relation[18]:

$$\begin{aligned}\Delta n_r(\lambda_0, F) &= \frac{\lambda_0^2}{2\pi^2}P\int_0^\infty \frac{\Delta\alpha(\lambda, F)}{\lambda_0^2 - \lambda^2}\mathrm{d}\lambda \\ &= \frac{\lambda_0^2}{2\pi^2}\left[\lim_{\varepsilon\to 0}\int_0^{\lambda_0-\varepsilon}\frac{\Delta\alpha(\lambda, F)}{\lambda_0^2 - \lambda^2}\mathrm{d}\lambda\right. \\ &\quad \left. + \lim_{\varepsilon\to 0}\int_{\lambda_0+\varepsilon}^\infty \frac{\Delta\alpha(\lambda, F)}{\lambda_0^2 - \lambda^2}\mathrm{d}\lambda\right],\end{aligned} \tag{11}$$

where $P$ stands for the Cauchy principal value and $F$ is the electric field. The chirp parameter depends only on the electroabsorption material and not on the waveguide structure[19].

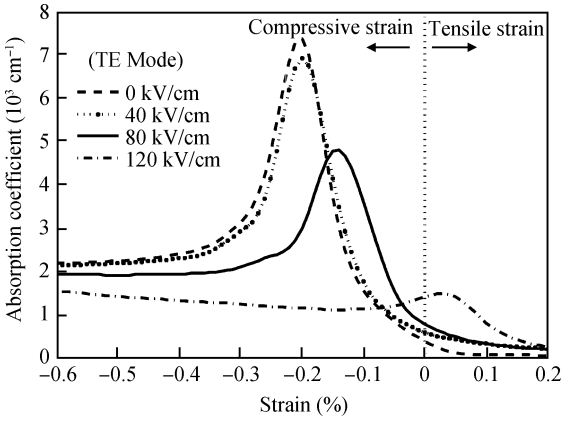


Fig. 2. Absorption coefficient as a function of left well layer strain at $\lambda = 1.55$ $\mu$m.

Therefore, knowledge of the absorption spectrum of the EAM is required for characterizing the chirp parameter and frequency chirp. Since the chirp parameter is related to the slope of refractive index change versus absorption coefficient change curve, a negative chirp parameter is achieved with negative sign of the refractive index change and a positive sign of the absorption coefficient change, or vice-versa. Thus, the basis of an approach to achieve negative signs in the refractive index change and the chirp parameter lies in varying the shape of the electroabsorption spectra.

## 5. The insertion loss parameter

The insertion loss of EAM is composed of three sections, such as reflection loss at the facets, coupling loss from/to the optical fiber, and optical propagation loss. Propagation loss is the main contributor to insertion loss. It mainly depends on waveguide scattering loss, free carrier absorption loss and EA material residual absorption loss[20]. Insertion loss due to residual absorption, IL, is given by

$$\mathrm{IL} = 4.343\Gamma\alpha_0 L \ (\mathrm{dB}), \tag{12}$$

where $\alpha_0$ is the static electroabsorption coefficient in the ON state. The insertion loss increases very quickly as the waveguide length increases. Values of IL up to 2.5 dB are desirable for electroabsorption optical modulators.

## 6. Numerical simulation results and discussion

In the present section, firstly we examine the effect of strain in the left well layer from compressive to tensile, with a fixed right well strain of –0.52% (CS) on the chirp parameter and insertion loss in EAMs with an AICD-SQW active layer for different values of applied electric field ($F$) between 0 and 120 kV/cm at $\lambda = 1.55$ $\mu$m. For this purpose, the electroabsorption coefficient has been calculated. Figure 2 illustrates the strain dependence of the absorption coefficient for TE input light polarization. In the figure, an increase in the electric field decreases the peak value of the absorption coefficient and shifts the peak position towards the tensile strain side. The tensile strain of the left well layer enhances the absorption in higher electrical fields.

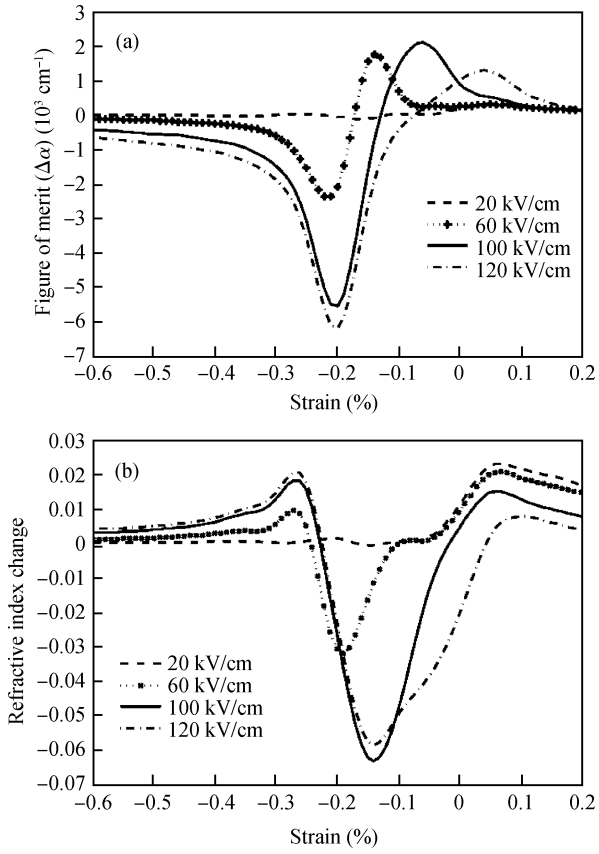


Fig. 3. (a) Calculated absorption coefficient changes, $\Delta\alpha$. (b) Calculated refractive index changes, $\Delta n_{\mathrm{r}}$, as a function of the left well layer strain at $\lambda = 1.55$ $\mu$m.

The $\Delta\alpha$ as a function of the left well layer strain at $\lambda = 1.55$ $\mu$m was obtained from the calculated absorption curves for different values of the applied electric field by subtracting its values for different electrical fields from that for the lowest non zero electrical field. Figure 3(a) shows the absorption coefficient changes, $\Delta\alpha$, of the AICD-SQW in the presence of applied electric fields. A large negative $\Delta\alpha$ can be seen at around 0.2% compressive strain (CS) due to the reduction in the oscillator strength for the lowest state subband excitons. Furthermore, the positive peak value of $\Delta\alpha$ moves towards the tensile strain side when the electric field increases. Once $\Delta\alpha$ is known, the change in the refractive index $\Delta n_{\mathrm{r}}$ is calculated by the Kramers–Kronig relation.

Figure 3(b) illustrates the calculated refractive index changes as a function of the left well layer strain. At strain values near –0.22% and from –0.05% to 0.05%, the refractive index change is extremely low (nearly zero) over all the applied electrical fields. Therefore, EAM at $\lambda = 1.55$ $\mu$m indicates a negative chirp parameter due to a negative sign of the $\Delta n_{\mathrm{r}}$ and a positive sign of the $\Delta\alpha$.

Figure 4 illustrates how $\Delta n_{\mathrm{r}}$ varies with $\Delta\alpha$ for different strain values of the left well layer at $\lambda = 1.55$ $\mu$m. We can see from this figure that, in the compressive values of the left well layer strain, both $\Delta\alpha$ and $\Delta n_{\mathrm{r}}$ become negative (Fig. 4(a)). But for the tensile strain values, as $\Delta\alpha$ increases, $\Delta n_{\mathrm{r}}$ decreases. Eventually, $\Delta n_{\mathrm{r}}$ becomes negative (Fig. 4(b)).

From the $\Delta n_{\mathrm{r}}$ versus $\Delta\alpha$ curve, the chirp parameter $\alpha_{\mathrm{H}}$

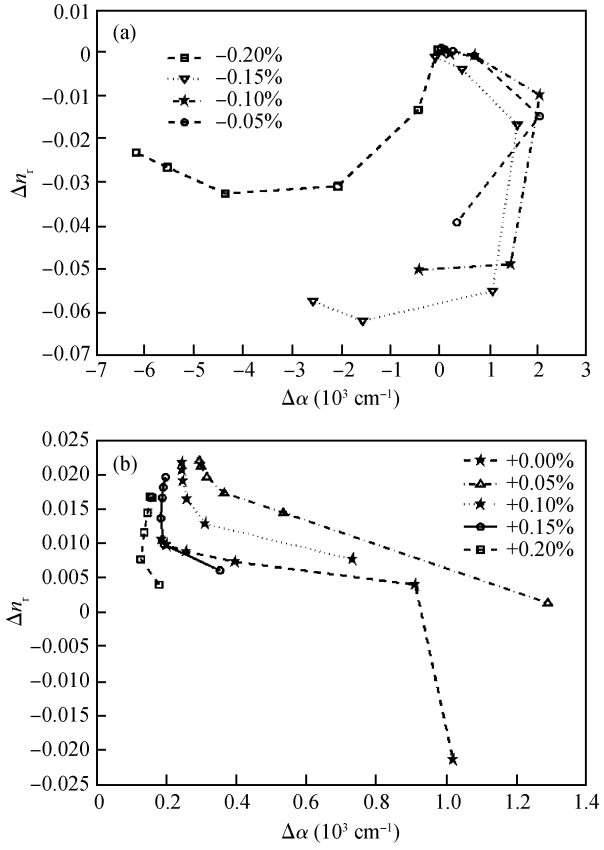


Fig. 4. (a) $\Delta n_r$ versus $\Delta\alpha$ for different compressive strain values. (b) $\Delta n_r$ versus $\Delta\alpha$ for different tensile strain values of the left well layer at $\lambda = 1.55$ $\mu$m.

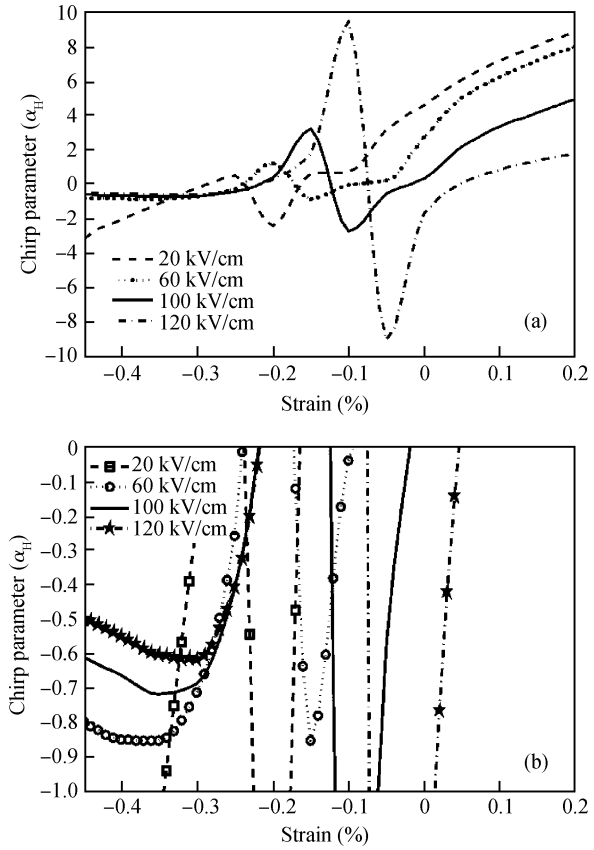


Fig. 5. (a) Chirp parameter $\alpha_H$ versus left well layer strain at $\lambda = 1.55$ $\mu$m for different values of applied electric field. (b) An enlarged image of Fig. 5(a).

can be obtained by using Eq. (10). The $\alpha_H$ is relative to the slope of the $\Delta n_r$ versus $\Delta\alpha$ curve. Figure 5 illustrates the calculated chirp parameters of the EAMs with the AICD-SQW as a function of the left well layer strain at $\lambda = 1.55$ $\mu$m. The negative values of the chirp parameter can be achieved over a range of the left well layer tensile strain from 0.02% to 0.05% for a 120 kV/cm value of applied electric field (Fig. 5(b)).

Figure 6 shows the calculated insertion loss as a function of the left well layer strain at $\lambda = 1.55$ $\mu$m. It is evident from this figure that, in the tensile values of the left well layer strain above 0.032%, insertion loss becomes very low, less than 2.5 dB. Since values of insertion loss up to 2.5 dB are desirable for electroabsorption optical modulators, a left well layer tensile strain above 0.032% will be very suitable for EAM with very low insertion loss. As a result, the best range of the left well strain for EAM based on AICD-SQWs with negative chirp and very low insertion loss will be from 0.032% to 0.05% (TS).

Now we investigate the influence of strain in the right well layer from compressive to tensile with a fixed left well strain of 0.05% (TS) on the chirp parameter and an insertion loss in EAMs with an AICD-SQW active layer for different values of applied electric field ($F$) between 0 and 120 kV/cm at $\lambda = 1.55$ $\mu$m.

Figure 7 illustrates the calculated chirp parameters of EAMs with the AICD-SQW as a function of the right well layer strain at $\lambda = 1.55$ $\mu$m. As we can see, the negative values of the chirp parameter can be achieved over a range of the right well layer strain from –0.52% (CS) to 0.1% (TS) for a 120 kV/cm

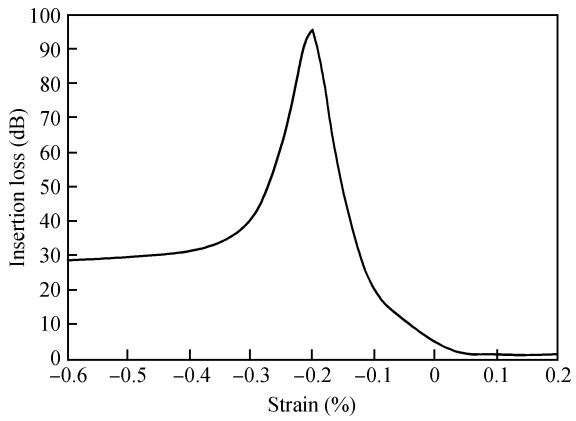


Fig. 6. Calculated insertion loss versus left well layer strain at $\lambda = 1.55$ $\mu$m for different values of applied electric field.

value of applied electric field.

Figure 8 shows the calculated insertion loss as a function of the right well layer strain at $\lambda = 1.55$ $\mu$m. It is evident from this figure that over a range of the right well layer compressive strain from –0.88% to –0.50%, insertion loss becomes low, less than 2.5 dB. Furthermore, we see that the insertion loss increases very quickly as the value of the right well strain decreases. Therefore, it is determined that the best range of the right well strain for EAM based on AICD-SQW with negative chirp and very low insertion loss will be from –0.52% to

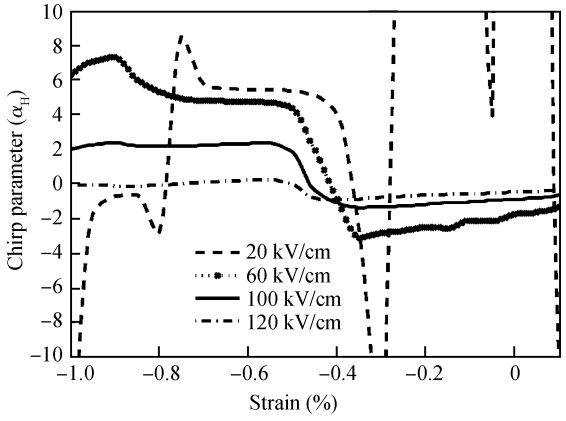


Fig. 7. Chirp parameter $\alpha_H$ versus right well layer strain at $\lambda = 1.55$ $\mu$m for different values of applied electric field.

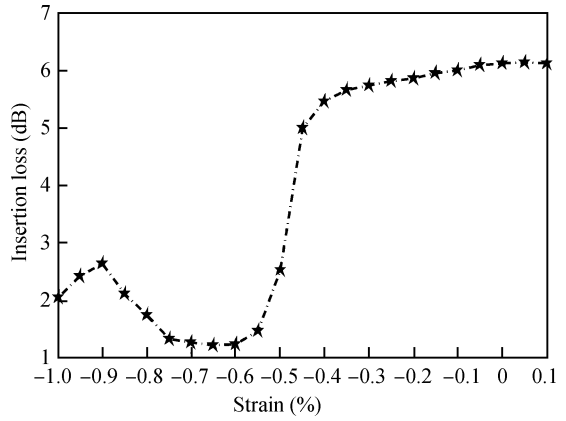


Fig. 8. Calculated insertion loss versus right well layer strain at $\lambda = 1.55$ $\mu$m.

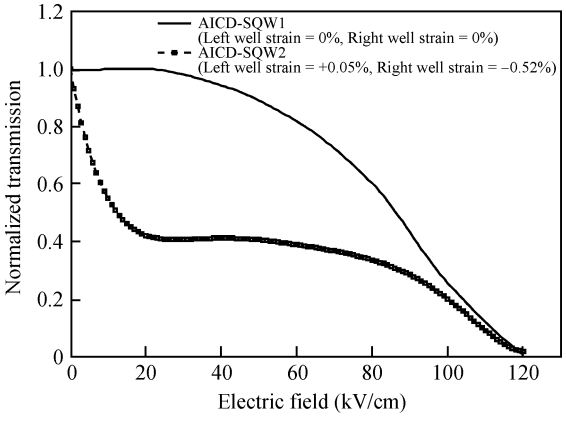


Fig. 9. Calculated normalized transmission versus applied electric field at $\lambda = 1.55$ $\mu$m.

–0.50% (CS).

Figure 9 indicates the estimated normalized transfer curves of the EAMs for two AICD-SQW structures. In the AICD-SQW1 structure, the well layers have zero strain. The left and right wells of the AICD-SQW2 structure contain 0.05% tensile and 0.52% compressive strain, respectively.

## 7. Conclusion

In this paper, EAMs with negative chirp and very low insertion loss were numerically designed with an AICD-SQW active layer based on InGaAlAs material. The electroabsorption coefficient was calculated over a range of AICD-SQW strain from compressive to tensile. The chirp parameters and insertion loss for TE input light polarization were evaluated from the calculated electroabsorption spectra and their Kramers–Krönig transformed refractive index changes. The results of the numerical simulation showed that the best range of the left and right wells strain for EAM based on AICD-SQWs with negative chirp and very low insertion loss are from 0.032% to 0.05% (TS) and –0.52% to –0.50% (CS), respectively.

## Acknowledgements

The author would like to express his gratitude to Professor V. Ahmadi and Dr. E. Darabi for useful discussions.

## References

[1] Irmscher S, Lewén R, Eriksson U. InP/InGaAsP high-speed traveling-wave electro-absorption modulators with integrated termination resistors. IEEE Photonics Technol Lett, 2002, 14: 923

[2] Watanabe T, Sakaida N, Yasaka H, et al. Transmission performance of chirp-controlled signal by using semiconductor optical amplifier. J Lightwave Technol, 2000, 18: 1069

[3] Wakita K, Yoshino K, Kotaka I, et al. Blue-chirp electroabsorption modulators with very thick quantum wells. IEEE Photonics Technol Lett, 1996, 8: 1169

[4] Raring J W, Skogen E J, Johansson L A, et al. Widely tunable negative-chirp SG-DBR laser/EA-modulated transmitter. J Lightwave Technol, 2005, 23: 80

[5] Kato M, Touda R, Nakano Y. Control of chirp parameter in electroabsorption modulators by designing asymmetric triple coupled quantum well structure. Lasers and Electro-Optics CLEO/Pacific Rim, 1999, 3: 1046

[6] Guo C L, Sun C Z, Hao Z B, et al. Theoretical analysis of polarization insensitive InGaAsP multiple-quantum-wells eletroabsorption modulators with negative chirp. Jpn J Appl Phys, 2000, 39: 6166

[7] Trezza J A, Powell J S, Harris J S. Zero chirp asymmetric Fabry–Perot electroabsorption modulator using coupled quantum wells. IEEE Photonics Technol Lett, 1997, 9: 330

[8] Tada K, Arakawa T, Kazuma K, et al. Influence of one monolayer thickness variation in GaAs/AlGaAs five-layer asymmetric coupled quantum well upon electrorefractive index change. Jpn J Appl Phys, 2001, 40: 656

[9] Miyazaki Y, Tada H, Tokizaki S Y, et al. +1 dBm average optical output power operation of small-chirp 40-Gbps electroabsorption modulator with tensile-strained asymmetric quantum-well absorption layer. IEEE J Quantum Electron, 2003, 39: 1009

[10] Miyazaki Y, Tada H, Tokizaki S Y, et al. Small-chirp 40-Gbps electroabsorption modulator with novel tensile-strained asymmetric quantum-well absorption layer. IEEE J Quantum Electron, 2003, 39: 813

[11] Jamro M Y, Senior J M. Chirp control of an electroabsorption modulator to be used for regeneration and wavelength conversion at 40 Gbit/s in all-optical networking. Photonic Network Com-

munications, 2005, 10: 267
[12] Shin D S, Jeong H. Chirp parameter of electroabsorption modulators with InGaAsP intrastep quantum wells. Jpn J Appl Phys, 2005, 44: L590
[13] Abedi K, Ahmadi V, Darabi E, et al. Design of a novel periodic asymmetric intra-step-barrier coupled double strained quantum well electroabsorption modulator at 1.55 $\mu$m. Solid-State Electron, 2008, 53: 312
[14] Abedi K, Ahmadi V, Moravvej-Farshi M K. Optical and microwave analysis of mushroom-type waveguides for traveling wave electroabsorption modulators based on asymmetric intra-step-barrier coupled double strained quantum wells by full-vectorial method. Opt Quant Electron, 2009, 41: 719
[15] Abedi K. Improvement of saturation optical intensity in electroabsorption modulators with asymmetric intra-step-barrier coupled double strained quantum. Eur Phys J Appl Phys, 2011, 56: 10403
[16] Zhang Wei, Pan Jiaoqing, Zhu Hongliang, et al. High-performance electroabsorption modulator. Journal of Semiconductors, 2009, 30: 094008
[17] Koyama F, Iga K. Frequency chirping in external modulators. IEEE J Lightwave Technol, 1988, 6: 87
[18] Yamanaka T, Wakita K, Yokoyama K. Potential chirp-free characteristics (negative chirp parameter) in electroabsorption modulation using a wide tensile-strained quantum well structure. Appl Phys Lett, 1996, 68: 3114
[19] Dorgeuille F, Devaux F. On the transmission performances and the chirp parameter of a multiple-quantum-well wlectroabsorption modulator. IEEE J Quantum Electron, 1994, 30: 2565
[20] Pires M P, Souza P L, Yavich B, et al. On the optimization of InGaAs–InAlAs quantum-well structures for electroabsorption modulators. J Lightwave Technol, 2000, 18: 598